drones

MDPI

Article

Cooperative Joint Mission Between Seismic Recording and Surveying UAVs for Autonomous Near-Surface Characterization

Jory Alqahtani [1,*], Ahmad Ihsan Ramdani [1], Pavel Golikov [1], Artem Timoshenko [2], Grigoriy Yashin [2], Ilya Mashkov [2], Van Do [3] and Ezzedeen Alfataierge [1]

[1] EXPEC Advanced Research Center Saudi Aramco, Dhahran 31311, Saudi Arabia; ahmad.ramdani@aramco.com (A.I.R.); pavel.golikov@aramco.com (P.G.); ezzedeen.alfataierge@aramco.com (E.A.)
[2] Aramco Research Center-Moscow, Aramco Innovations LLC, 117105 Moscow, Russia; artem.timoshenko@aramcoinnovations.com (A.T.); grigoriy.yashin@aramcoinnovations.com (G.Y.); ilya.mashkov@aramcoinnovations.com (I.M.)
[3] Geophysical Imaging Department Saudi Aramco, Dhahran 31311, Saudi Arabia; van.do@aramco.com
* Correspondence: jory.alqahtani.1@aramco.com or joryq@outlook.com

Highlights

What are the main findings?

- The integration of autonomous Unmanned Aerial Vehicles (UAVs) into land seismic data acquisition enables high-resolution aerial scouting followed by efficient seismic data collection.
- The cooperative system of Scouting UAV and Autonomous Seismic Acquisition Device (ASAD) can acquire high-resolution seismic data comparable to conventional data acquisition systems, with a superior frequency bandwidth suitable for imaging shallow anomalies.

What are the implications of the main finding?

- The proposed system can complement seismic data acquisition by enhancing safety, increasing productivity, and decreasing logistical challenges, while minimizing environmental footprint.
- The system has potential for near-surface characterization and shallow geohazard identification, as demonstrated by its accurate detection of a shallow subsurface cavity.

Abstract

Generally, land seismic data acquisition in arid areas is a labor-intensive, costly, and challenging process, often hindered by challenging terrain and safety risks. To overcome these limitations, we propose the integration of autonomous Unmanned Aerial Vehicles (UAVs) into land seismic data acquisition, enabling efficient data collection in difficult, inaccessible terrain. This is a cooperative mission workflow combining a Scouting UAV for high-resolution aerial scouting, followed by the swarm deployment of an Autonomous Seismic Acquisition Device (ASAD) for seismic data recording. The cooperative system allows for precise landing and subsequent deployment of seismic sensors in optimal locations. Previously, we demonstrated the applicability of passive seismic recorded with ASAD drones to near-surface characterization. This study covers the results of a field trial, where both the ASAD and Scouting UAV systems successfully acquired high-resolution seismic data with an active source, comparable to that of a conventional seismic data acquisition system. The results show that the ASAD seismic data exhibit a slightly higher noise level due to coupling variances and the fact that geophones were hardwired into 9-sensor arrays. However, due to its single-point sensing nature, it yields a superior frequency

Check for updates

Academic Editors: Bastien Dupuy, Filippo Accomando, Piyoosh Jaysaval, Yuxin Wu and Pablo Rodríguez-González

Received: 26 February 2026
Revised: 3 April 2026
Accepted: 9 April 2026
Published: 14 April 2026

Copyright: © 2026 by the authors. Licensee MDPI, Basel, Switzerland. This article is an open access article distributed under the terms and conditions of the Creative Commons Attribution (CC BY) license.

bandwidth, making it suitable for imaging shallow anomalies. The system underwent P-wave refraction tomography modeling and accurately detected a shallow subsurface cavity, showcasing its potential for near-surface characterization and shallow geohazard identification. This heterogeneous robotic system can support seismic data acquisition by enhancing safety, improving efficiency, and streamlining equipment mobilization, while minimizing environmental footprint.

Keywords: field robots; seismic data acquisition; site reconnaissance; swarm robotics; unmanned aerial vehicle (UAV); UAV mapping; remote sensing

1. Introduction

Seismic imaging methods provide critical insights into the subsurface for a diverse range of applications, including hydrocarbon exploration, civil engineering, near-surface geohazard detection, and earthquake hazard assessment [1–3]. The fundamental principle involves generating seismic waves and recording their propagation through the Earth using an array of sensors (geophones or accelerometers). The resulting data yield detailed images of subsurface structures and physical properties. However, the fidelity of these images is intrinsically linked to the quality, density, and spatial distribution of the acquired data [4–7].

Conventional land seismic data acquisition in arid areas remains profoundly labor-intensive, costly, and challenging. It requires acquisition crews to manually deploy hundreds or thousands of sensors across often inaccessible terrain (Figure 1A,B), including arid deserts, steep mesas, unstable slopes, and karstified regions [8,9]. This manual process not only imposes significant HSE risks but also creates economic and sustainability limitations. Accessibility and safety concerns inevitably lead to gaps in survey coverage, as certain areas are deemed too difficult to access. This limitation may result in incomplete datasets and potential ambiguities in data interpretation [5,6,9]. Furthermore, pre-acquisition seismic survey planning has traditionally relied on satellite data [10,11]. While these datasets offer extensive coverage, they often lack the resolution and timeliness needed to identify recent obstacles, subtle terrain variations, or optimal sensor placements. These limitations lead to inefficiencies and suboptimal source-receiver geometries on-site, especially for high-resolution, dense acquisition [7,12].

In response to these challenges, the integration of Unmanned Aerial Vehicles (UAVs) into geophysical data acquisition has emerged as a transformative technological frontier. The concept of leveraging UAVs for seismic data acquisition in unsafe and inaccessible terrain promises to mitigate risks, reduce costs, and access logistically complex areas. Initial systems, such as the METIS project, demonstrated the potential of UAVs to air-drop sensor nodes across a survey area [13,14]. More recently, the scope of UAV geophysics has expanded and now may include multimodal sensor fusion [15,16]. This system enables a single mission to integrate high-precision magnetometry, gravimetry, and electromagnetic (EM) sensors to provide a holistic subsurface model [15,16]. Recent studies have highlighted the use of UAV-towed scalar magnetic gradiometry for mineral exploration in extreme environments, demonstrating that lightweight, low-power sensors can now achieve the resolution previously reserved for ground-based arrays [17]. Furthermore, contemporary advancements have enabled AI-driven motion planning and "vision-based" sensing [18]. This system may enable UAVs to autonomously navigate complex vertical topographies and identify optimal geophone coupling points in real time.



Figure 1. An example of a land seismic data acquisition crew camp (**A**) and geophone arrays (**B**), highlighting the labor-intensive nature and challenges of deploying sensors in desert terrain. (**C**) ASAD is a UAV equipped with a mechanism for deploying a package of seismic sensors.

While air-dropping sensors remains an innovative approach, it offers no flexibility for sensor repositioning/adjustment once deployed. A more robust solution involves UAVs capable of precise landing to deploy seismic sensors and record seismic data from the ground [19–21]. UAV, like Autonomous Seismic Acquisition Device (ASAD) [19], ensures high-quality data acquisition and allows for flexible, adaptive survey designs (Figure 1C). The swarm of seismic drones can collect either passive seismic data when an active source is available or active data with vibroseis or any other type of active source. The benchmarking of data recording quality by ASAD seismic sensors and traditional recording systems has been experimentally demonstrated in a series of studies [19,21]. Concurrently, the use of UAVs equipped with cameras for high-resolution aerial photogrammetry has become a standard tool for rapid site reconnaissance. These systems can generate cm-scale digital elevation models (DEMs) and orthomosaics, providing a high-resolution, up-to-date view of the terrain for geoscience data acquisition and reconnaissance [7]. The logical advancement is the seamless integration of these two capabilities into a single, cooperative ecosystem.

The general objective of this study is to demonstrate the results of a field trial of a cooperative joint mission between two specialized UAVs: an Autonomous Seismic Acquisition Device (ASAD) and an aerial photogrammetry UAV. This integrated system serves as a proof-of-concept for a lightweight, fully autonomous land-based seismic data-acquisition and reconnaissance crew. The specific objectives are fourfold:

1. Describe the architecture and capabilities of the cooperative UAV system.
2. Outline the autonomous workflow from photogrammetric reconnaissance to seismic data recording in a controlled field environment.

3. Validate the performance of the ASAD's integrated seismic sensor through a direct comparison of raw data and processed seismic refraction tomograms against those measured by a conventional, co-located geophone.
4. Discuss the performance of the tested system and future development directions of fully autonomous geophysical operations based on field experimental results.

2. Description of the Test Site and the UAVs

2.1. Field Site Description

We conducted the trial in a dedicated outdoor test facility (Figure 2A). The controlled field environment is a secure, fenced area measuring approximately 200 m by 650 m. The size of the area was specifically calculated to allow for the deployment of UAV swarms with sufficient buffer zones for safe take-off, landing, and localized maneuvering. Geophysically, the size of the test area is also adequate for a meaningful seismic refraction analysis [1]. The test site's surface conditions are a mix of natural desert terrain and anthropogenic infrastructure, representing the "standard urban setting" encountered in arid desert environments (Figure 2B). The environment includes sparse vegetation, buildings, gravel, rocks, anthropogenic debris, service roads, and localized sand deposits. These features pose challenges for the ASAD swarms, as they must navigate around surface obstacles before landing and recording data. The presence of loose soil and sand at the surface also tests the mechanical coupling capabilities of ASAD's seismic sensor payload.



Figure 2. Overview of the controlled field test environment. (**A**) Satellite image of the dedicated outdoor test facility, exhibiting a "standard urban setting" mix of natural desert terrain and anthropogenic infrastructure. Satellite data presented is from World Imagery [22]. (**B**) Example view of surface conditions, including loose soil and sand deposits that test the mechanical coupling of the ASAD. (**C**) The artificial geohazard experiment setup, showing a vertically buried industrial barrel located 2 m below the surface to simulate a near-surface cavity.

2.2. Artificial Shallow Cavity Detection Experiment

Shallow cavities are typical in carbonate layers in arid environments [23–26]. These cavities pose significant challenges for field operations. Therefore, robust methods for the detection of such cavities are very important. As part of a controlled experiment, an artificial shallow subsurface cavity at the test site was planted to simulate the ASAD's

applicability for identifying shallow near-surface geohazards, a feature that is difficult to image with sparse conventional seismic grids [24,26]. The artificial cavity is a vertically buried steel barrel located 2 m below ground surface (Figure 2C). The barrel acts as a distinct impedance contrast against the surrounding soil matrix, representing a void from a localized karst dissolution feature. The roof of a cavity often gradually collapses [27,28], creating a local zone of reduced density and velocity that propagates upward. To replicate this feature, we covered the barrel with loose soil. This deterministic setup allows for a definitive evaluation of the ASAD system. Since the exact location and dimensions of the target are known, any artifacts or positioning errors of the barrel can be directly attributed to the experiment setup rather than geological uncertainty.

2.3. Description of Integrated System for Seismic Reconnaissance and Data Acquisition

The developed system includes three main components: the scouting UAV, a group of UAVs equipped with seismic sensors (named ASADs), and a Swarm control station (SCS) located on the ground. ASAD is a robotic platform with the recording capabilities of a terrestrial seismic sensor [19,21]. SCS provides a high-level control of the system with developed flight planning and control software (FPCS). It generates task lists for the robots based on the operators' setups and target locations for recorders. Also, SCS provides wireless communication with robots, mission monitoring, and direct control of robot subsystems. Upon receiving a task list from the SCS, ASAD executes an acquisition mission autonomously, takeoff, flight, landing in a target position, sensor coupling, and signal recording. The Scouting UAV is a quadrotor equipped with a high-resolution camera. This UAV performs its reconnaissance mission along a path set by the operator to cover the entire area of interest.

2.3.1. Autonomous Seismic Acquisition Device (ASAD)

The ASAD is a quadrotor-based robotic platform that integrates standard UAV flight capabilities with a specialized system for autonomous seismic data recording (Figure 3) [19]. Its architecture comprises four key subsystems: the airframe and avionics, an onboard computer (OBC), a Sensor Deployment System (SDS), and an On-board Data Acquisition Module (ODAM).

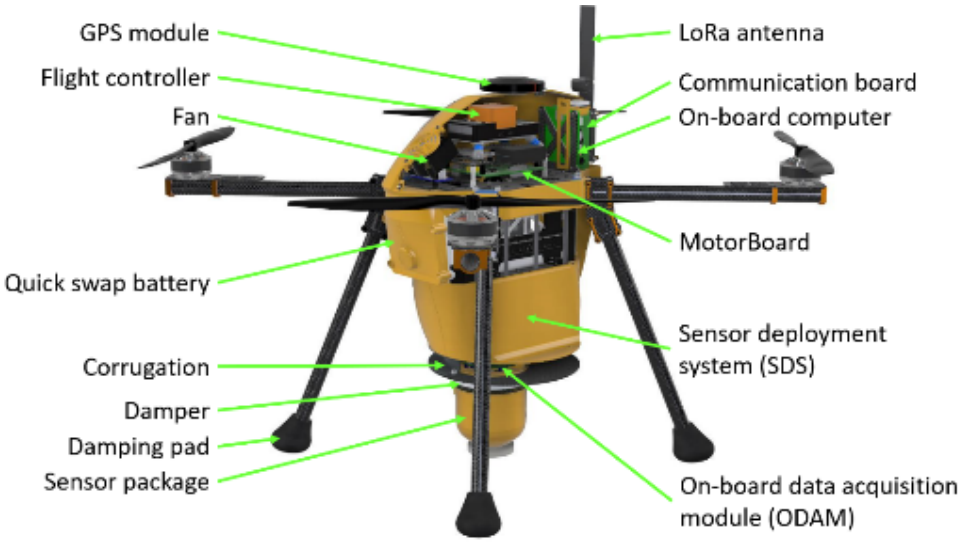

Figure 3. The layout of ASAD [21].

The core of the ASAD control system is the on-board computer (OBC). The OBC centralizes control of all ASAD's subsystems using the Robot Operating System (ROS) framework. Each software module is responsible for its own subsystem and implements all the OBC functionality:

- Communication with the SCS, receiving commands and task files, switches cooling fans for temperature control, and transmitting the robot's telemetry via Wi-Fi and LoRa by using a custom-developed communication board;
- Flight control, interaction with the flight controller, task file processing, tracking, and executing autonomous missions based on the task file;
- Control of the SDS via its own motor control board (MotorBoard);
- Connection and management of the system for recording sensor data, implemented in a separate board, ODAM.

In addition to the functions described above, the OBC performs diagnostics of the subsystems to avoid hazardous situations and notifies the system operator of any detected malfunctions.

The SDS enables sensor-ground coupling. Upon landing at a target point, the SDS lowers the sensor package and presses it to the ground using the robot's own weight. Seismic signal recording is performed by the ODAM, which comprises geophones and MEM accelerators connected to a custom board with a microcontroller and ADCs. The sensors convert incoming seismic waves (mechanical ground motion) into impedance changes; the ADC digitizes the results into an electrical signal, and the microcontroller streams the digitized data to the on-board computer at 2000 samples per second for file storage.

2.3.2. Swarm: Control Station (SCS)

For communication, the SCS employs a dual-link strategy (Figure 4). A Wifi-Link (2.4/5 GHz) provides high-bandwidth file exchange (e.g., task lists, recorded seismic data) over a limited range (50–100 m). A separate LoRa radio link (433 MHz) supports low-bandwidth, long-range (up to 10 km) telemetry for diagnostics and basic control commands (e.g., mission abort, deploy/undeploy sensor, set new times, etc.). This dual approach balances data throughout needs with operational safety and flexibility in complex exploration environments where radio transmission may be degraded by physical obstacles and terrain irregularities.

2.3.3. Flight Planning and Control Software (FPCS)

FPCS is a custom-developed application that includes a set of functions for safe and successful autonomous communication with automated UAVs, planning and tracking flight trajectories, and robot behavior in a user-friendly and intuitive format [21]. The FPCS appearance is presented in Figure 5. Its functionality is organized into three components. First, the frontend provides operator situational awareness by displaying ASAD positions and telemetry on an interactive map. Second, the server-side component ensures reliable bidirectional data exchange, enabling command distribution and robot status collection. Third, the mission planner automates target assignment and route planning, generating collision-free trajectories based on user-defined parameters and robot states.

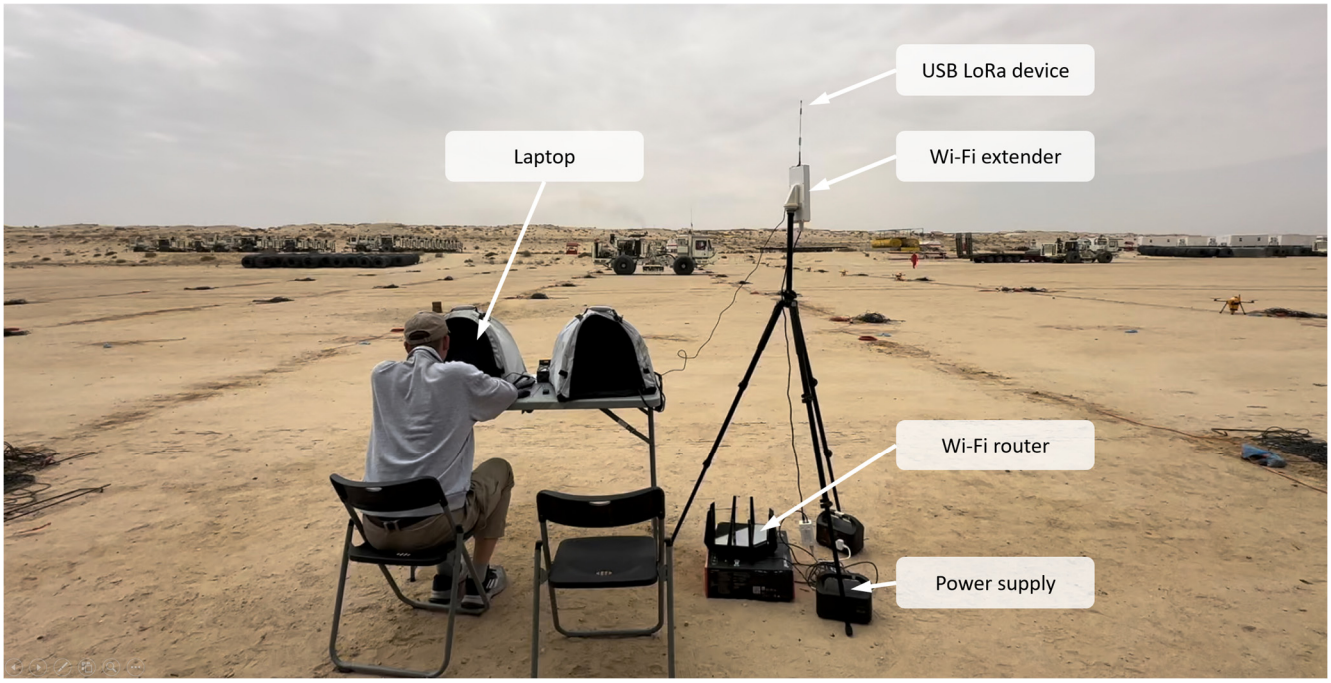

Figure 4. SCS during the 3D cross-spread survey.

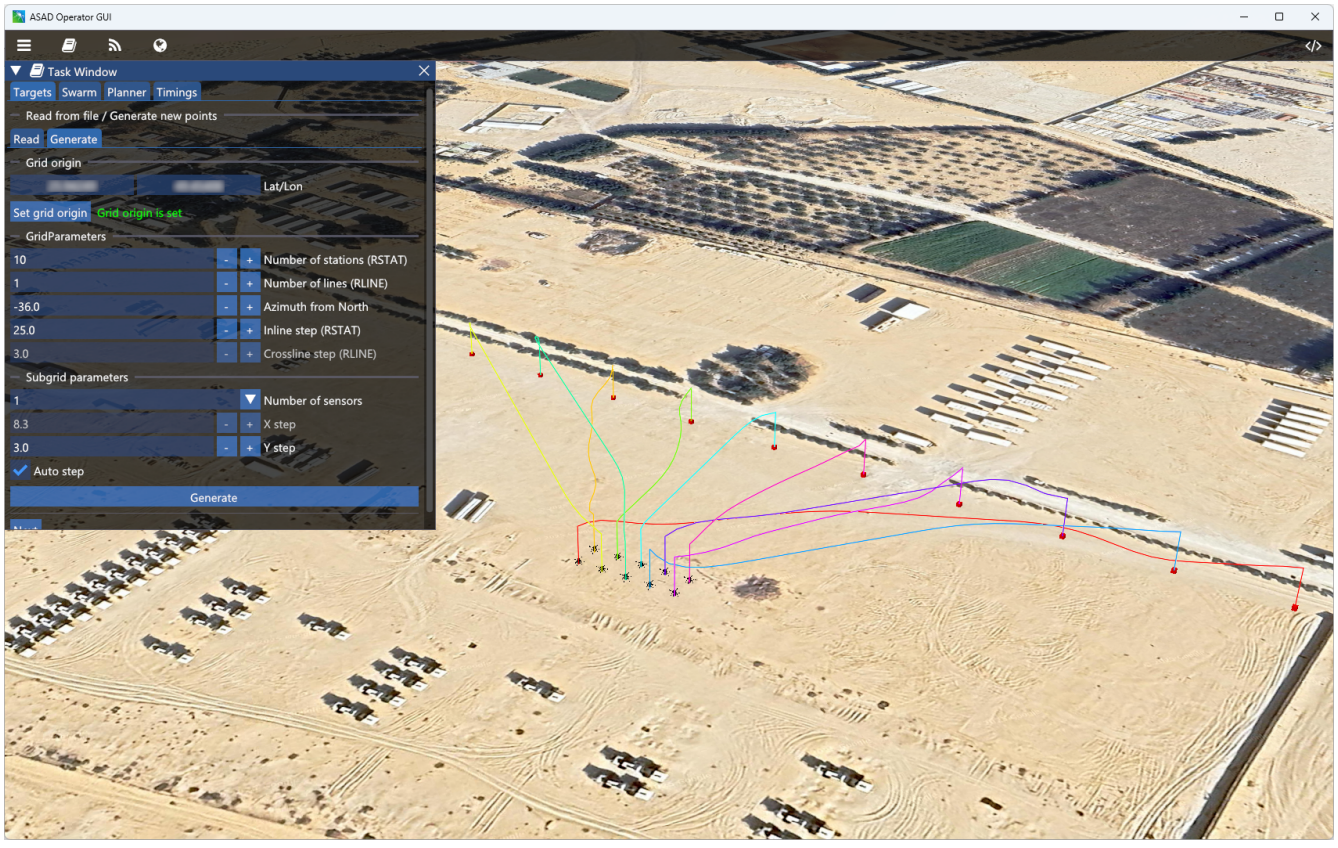

Figure 5. The FPCS appearance. An example mission for 10 ASADs with a single flight, with each UAV's trajectory highlighted in individual colors.

2.4. Scouting UAV

For efficiency and weight reduction, the ASAD lacks terrain surveying capabilities. However, the ASAD swarm does not fly blindly. Instead, it relies on a prior reconnaissance mission conducted by an aerial photogrammetry UAV. This Scouting UAV is tasked with generating a high-resolution 3D terrain model of the survey area. The model is then used to identify safe landing zones where the ASAD can land without tipping over. In this field trial, the Scouting UAV was built based on the ASAD body (Figure 6). Instead of the seismic payload, the Scout is equipped with a lightweight, 27-megapixel action camera. The camera shutter is synchronized with a GNSS logger. Every image captured is tagged with its precise geodetic coordinates (latitude, longitude, altitude) for photogrammetric processing.

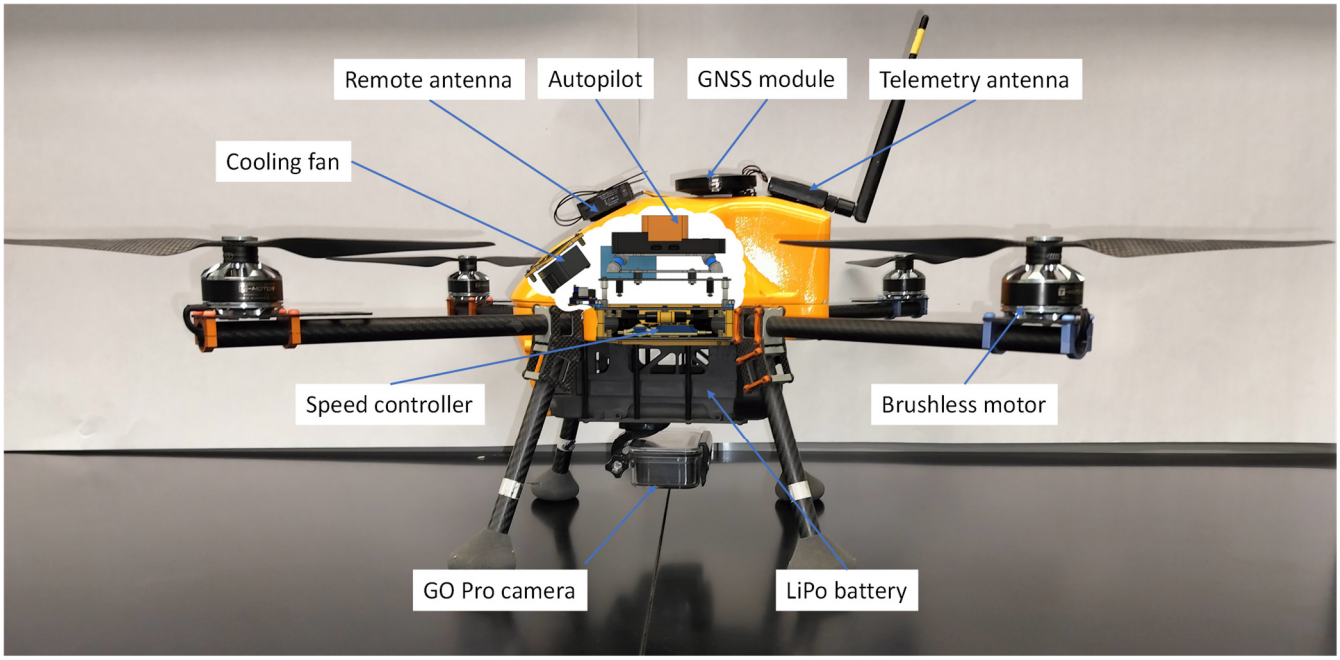

Figure 6. Scouting UAV, built on the same frame as the ASAD.

3. Cooperative Mission Workflow

The cooperative mission workflow between ASAD and Scouting UAV involves three sequential operations (Figure 7): reconnaissance, planning, and acquisition. In the reconnaissance stage, the Scouting UAV conducts an aerial photogrammetry survey to construct a high-resolution 3D terrain model of the test area. In the planning stage, the terrain model is converted into a semantic ASAD safe landing zones map. This information is then transferred into ASAD's onboard computer via a developed application named Flight Planning and Control System (FPCS). The terrain model is also used to optimize source-receiver geometry based on the elevation profile and actual ground conditions. During the acquisition stage, a swarm of ASADs autonomously acquires seismic data according to the pre-loaded mission plan. They take off from home position, fly to the designated recording point, check that the landing area is safe, land, deploy the sensor, and record the seismic data. Once recording is complete at a point, they retract the sensor, fly to the next recording point, and repeat until all points have been measured. Upon the acquisition mission's conclusion, the ASAD swarm returns home.

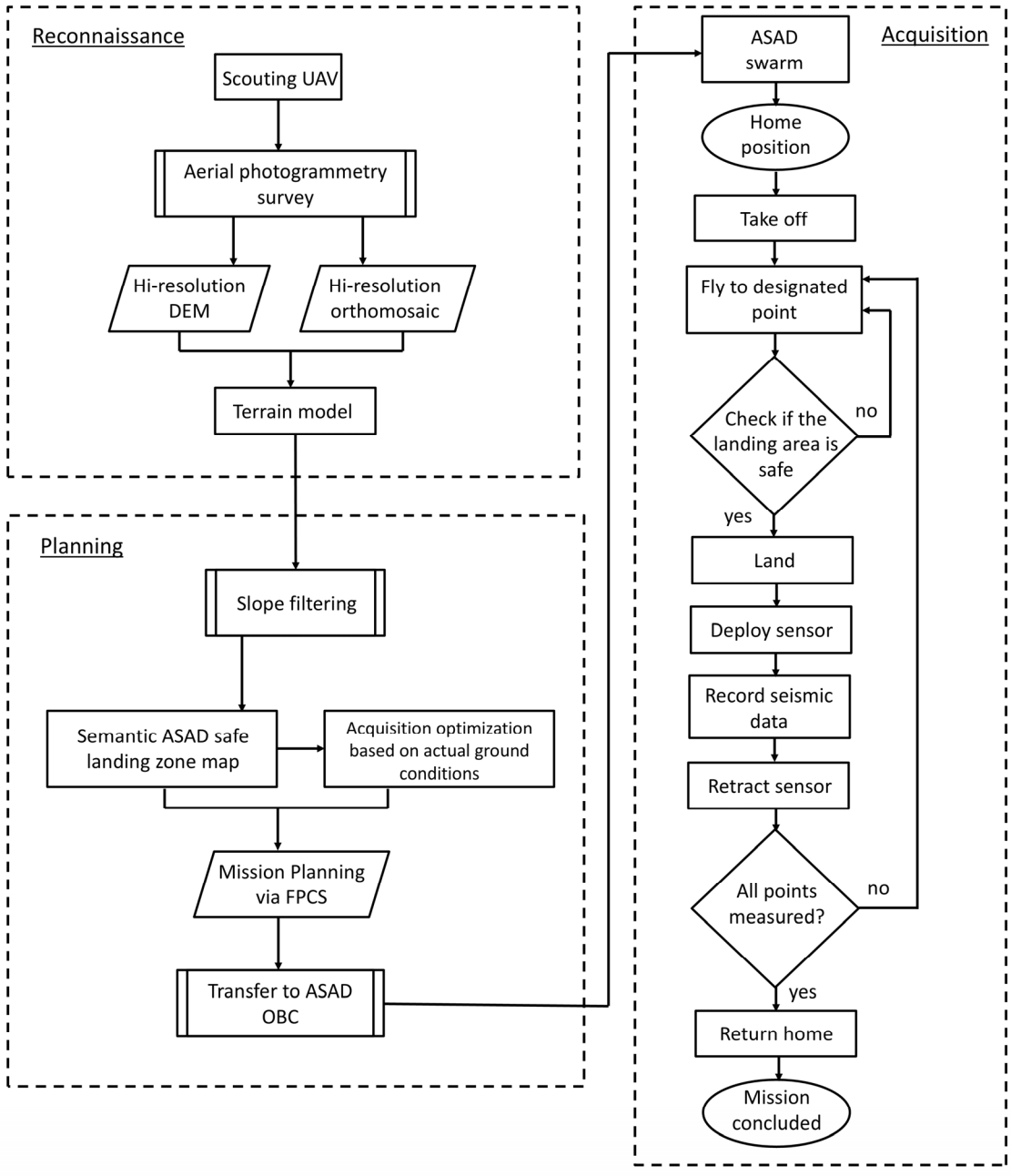

Figure 7. Cooperative mission workflow between Scouting-UAV and ASAD. The workflow consists of three stages: Reconnaissance, Planning, and Acquisition.

3.1. Reconnaissance Stage

We performed the scouting mission over the test area using a half-grid acquisition pattern (Figure 8A). The mission was flown at 40 m Above Ground Level (AGL). While the Scouting UAV can fly higher (up to ~100 m), a lower altitude was selected to maximize the Ground Sampling Distance (GSD). The ground speed was limited to 3 m per second (~10.8 km/h). This relatively slow speed prevents motion blur in the images and ensures the camera's write speed keeps up with the trigger interval. The mission maintained at least 80% overlap between adjacent photos. This high overlap is particularly important in desert terrains, where the lack of distinct visual features (textureless sand) can cause photogrammetry algorithms to fail if the view angle changes too rapidly between frames [29,30]. A single battery charge provides approximately 20–35 min of flight time. In a typical 20 min mapping mission at 40 m altitude, the system captures roughly 4000 images.

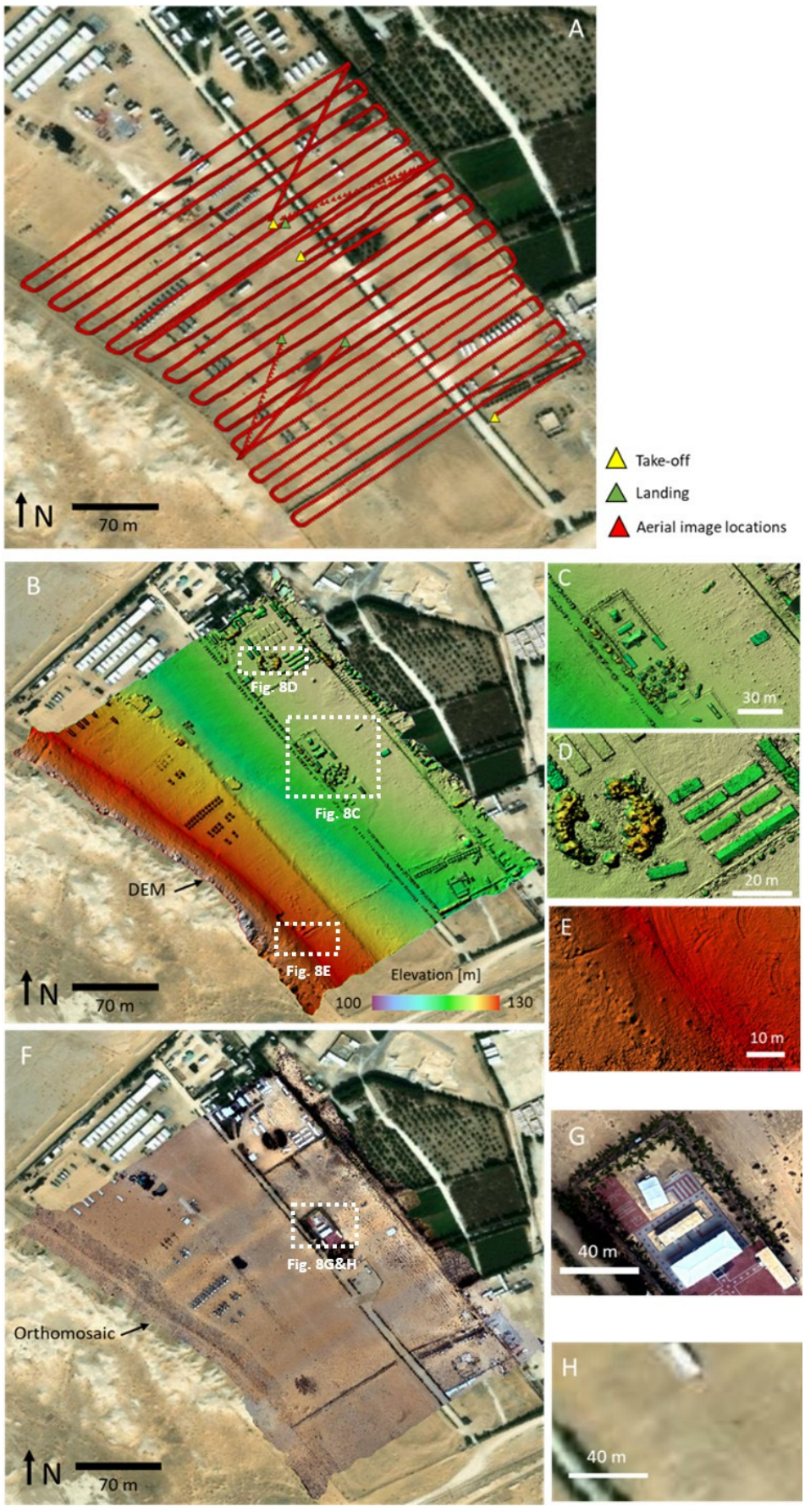

Figure 8. (**A**) The flight path of the Scouting UAV during the reconnaissance stage. (**B**) High-resolution Digital Elevation Model (DEMs of the test site were generated from the photogrammetric survey, with

a final resolution of 5 cm/pixel. (**C**,**D**) Examples of detailed objects resolved by the DEM that might be obstacles to the ASAD mission. (**C**) Areas with buildings and fences. (**D**) Areas with trees and warehouses. (**E**) Open space with gravel and boulders. (**F**) High-resolution orthomosaic images of the test field area, processed to a resolution of 1 cm/pixel. (**G**) An example of an orthomosaic image that shows an area with buildings and trees. These objects are absent in the satellite image (**H**) due to its much lower resolution and its lack of up-to-date information.

We tailored the photogrammetry processing workflow [31,32] to prioritize detecting small-scale hazards (such as rocks or bushes) that could endanger the ASAD during landing. Before processing, we filtered the dataset to remove images with high roll/pitch angles (taken during turns) or motion blur. Ground Control Points (GCPs), surveyed with RTK-GNSS on the ground, are identified in the images to "pin" the model to the absolute coordinate system [33]. Using GNSS tags as initial constraints, a bundle adjustment algorithm reconstructs the camera's positions and generates a sparse point cloud that represents the site's coarse geometry. We calculated a depth map for each image and fused them to create a 3D mesh, a digital elevation model (DEM), and an orthomosaic of the field test area. The final resolution of the DEM (Figure 8B–E) and orthomosaic image (Figure 8F–H) is 5 cm/pixel and 1 cm/pixel, respectively, with an accuracy of approximately 2 cm.

3.2. Planning Stage

The primary objective of the planning stage is to identify safe landing zones for the seismic ASAD swarm. The ASAD requires relatively flat, stable circular areas for touchdown and sensor coupling. Landing on a steep slope may exceed the UAV's mechanical stability limit and can result in a rollover. Thus, we performed slope filtering analysis based on the input DEM. For every pixel (i, j) in the DEM, the local surface normal vector n is computed. The slope angle θ is derived as the deviation of n from the vertical unit vector z. The mathematical formulation is

$$\theta_{i,j} = \cos^{-1}\left(n_{i,j} \cdot z\right)$$

The ASAD mechanical design imposes a strict operational limit. Field tests and simulations have established a critical slope threshold of 15°. We flag any cell in the DEM (within a 50 cm radius) with $\theta > 15^\circ$ as a "No-go Zone" for landing (Figure 9A,B). This conservative threshold accounts for the UAV's center of gravity when the sensor payload is deployed, preventing it from tipping over during the coupling phase. The No-Go Zone is then packaged into binary map data that is used during the preparation of target points for ASADs.

3.3. Acquisition Stage

The final stage involves the physical execution of the autonomous seismic acquisition by the ASAD swarm. It, in turn, can also be divided into several phases.

Preparatory phase. The ASADs are positioned on the launch pad at a safe distance from each other, either in a grid or randomly. The SCS is located on the nearest accessible elevated area near the robots' launch pad. All necessary devices are turned on: a router, a Wi-Fi extender, and a laptop with the software installed.

Connecting to the application. The server for connecting the robots is activated in the FPCS. The robots' batteries are turned on at the launch pad. As the robots power up, their onboard computers turn on and connect to the Wi-Fi network and, consequently, connect to the application server.

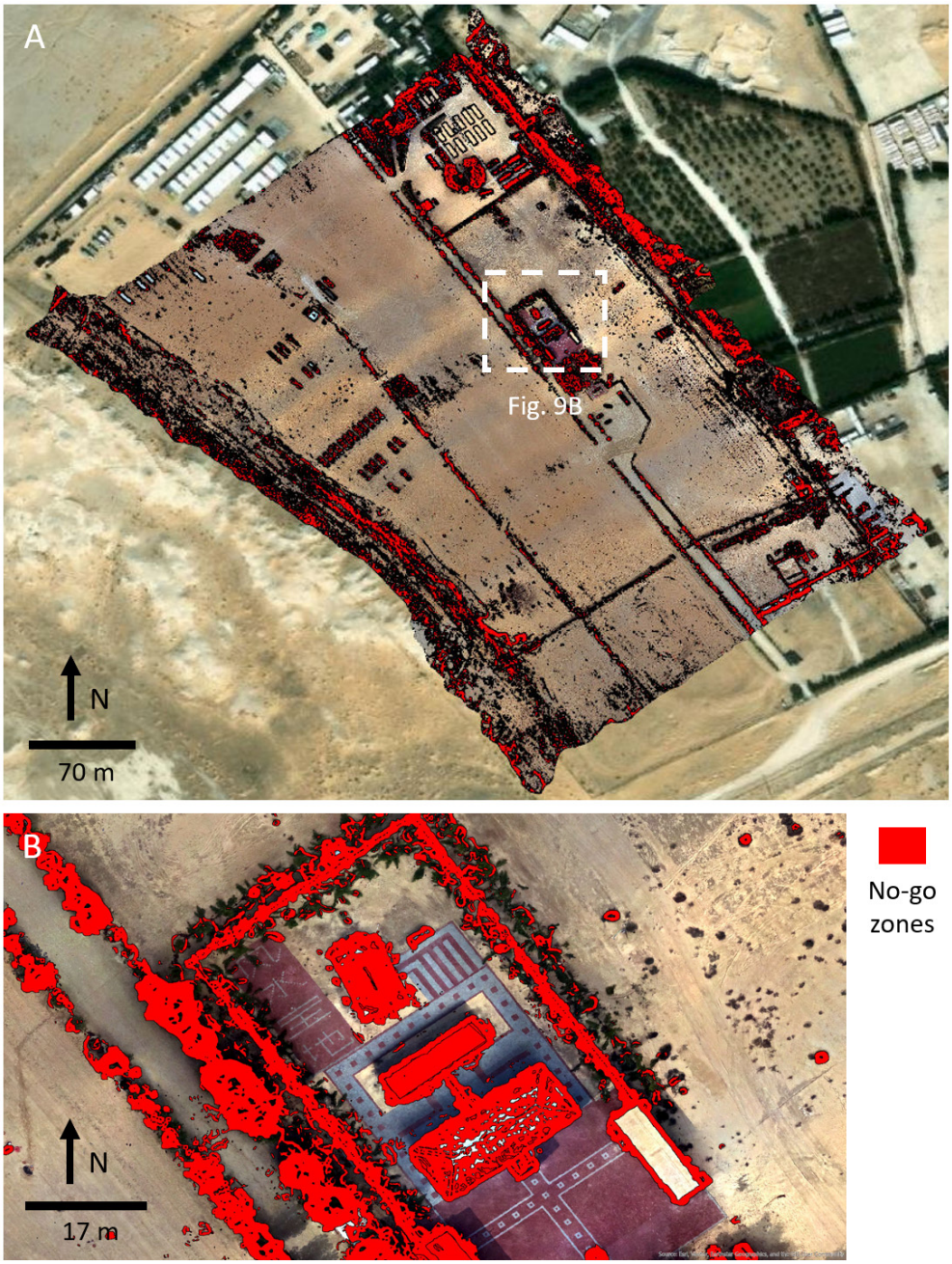

Figure 9. Safety analysis for autonomous landing. (**A**) Visualization of the ASAD "No-go Zone" derived from the DEM. Areas with a slope angle > 15 degrees are flagged (red) to prevent the ASAD from landing. (**B**) A zoom-in example that highlights part of the "No-go Zone" with buildings and trees.

Mission Parameters. The system operator specifies the target points where seismic signal measurements are to be performed. The FPCS allows for both options: specifying point coordinates from a file previously received from geophysicists or generating a grid of points directly on the map. When preparing a file with target points for ASADs, a map with marked areas is used. The target points are imported into the application with the "No-go Zones" removed. Recording duration and robotic system-specific parameters are also specified, including flight altitude and speed, maximum acceleration during takeoff and landing, and the spatial quantization resolution for the trajectory planner.

Trajectory Planning and Task File Distribution. After finalizing and validating all entered parameters, the operator launches the trajectory planner, which distributes target

points among the UAVs, plans the flight sequence, and generates task files for each ASAD. The operator visually checks the trajectory validity on the screen and decides whether to send the task files to the robots. Once the mission files are successfully sent to the ASADs, the team deactivates the kill switch on the robots, and they are ready to launch an autonomous mission.

Mission start. As soon as the mission start button is pressed, the corresponding command is sent via all available communication channels to the ASADs. The robots check key system states, confirming takeoff capability (GNSS accuracy, correct operation of the inertial measurement units, battery level, etc.). The robots perform all subsequent actions in accordance with the task list in the task file. The robots take off to the specified altitude. They then follow the flight path waypoints until the mission execution cursor reaches the landing task. Once all the robots have reached their destinations, they land.

Signal recording. After landing, each robot couples its sensor using the SDS. Signal recording starts on all robots synchronized with the mission start. When this task is activated, all robots begin recording the signal from the ODAM to a file on the OBC, having first turned off the cooling system fan to mitigate its effect on the seismic signal.

Mission continuation. After completing the ODAM signal recording, the robots move on to the next tasks on their task list. An autonomous mission can include multiple flights, in which case the cycle of takeoff, flight, landing, coupling, and data recording can be repeated. The mission can also end at the last recording point or include the UAV's return flight to the launch pad. If an abnormal situation, possibly a malfunction or an unsafe combination of circumstances, is detected, the operator can abort the mission and force the ASADs to land, either as a group or individually.

4. Seismic Data

4.1. Validation Setup

To validate ASAD's seismic data recording capability, we compared its measurements with those of conventional seismic acquisition systems. This validation setup utilized commercially available wireless nodes and conventional 10 Hz geophones (Figure 10A). Both the geophone and ASAD-UAV sensor specifications are shown in Table 1. In this experiment, we only used a few wireless nodes in certain locations. The geophones were co-located with ASAD acquisition points to ensure a direct comparison of the recorded wavefields. The experimental grid was structured with five source lines, each containing 40 source points, and five receiver lines, each containing 20 receiver points (Figure 10B). During operations, the ASAD swarm recorded data along a single receiver line before autonomously repositioning to the subsequent line. On the other hand, the conventional acquisition systems remained stationary at each designated station to provide a continuous baseline.

Table 1. Geophone sensor and ASAD specifications.

Characteristics	ASAD	Conventional Data Acquisition System	Wireless Node
Sensitivity, V/m/s	27.6	22.8	85.8
Natural Frequency, Hz	10	10	5
Sample rate, ms	8, 4, 2, 1, 0.5	8, 4, 2, 1	4, 2, 1, 0.5, 0.25
Allowable inclination angle, deg from vertical	≤20	<15	<15

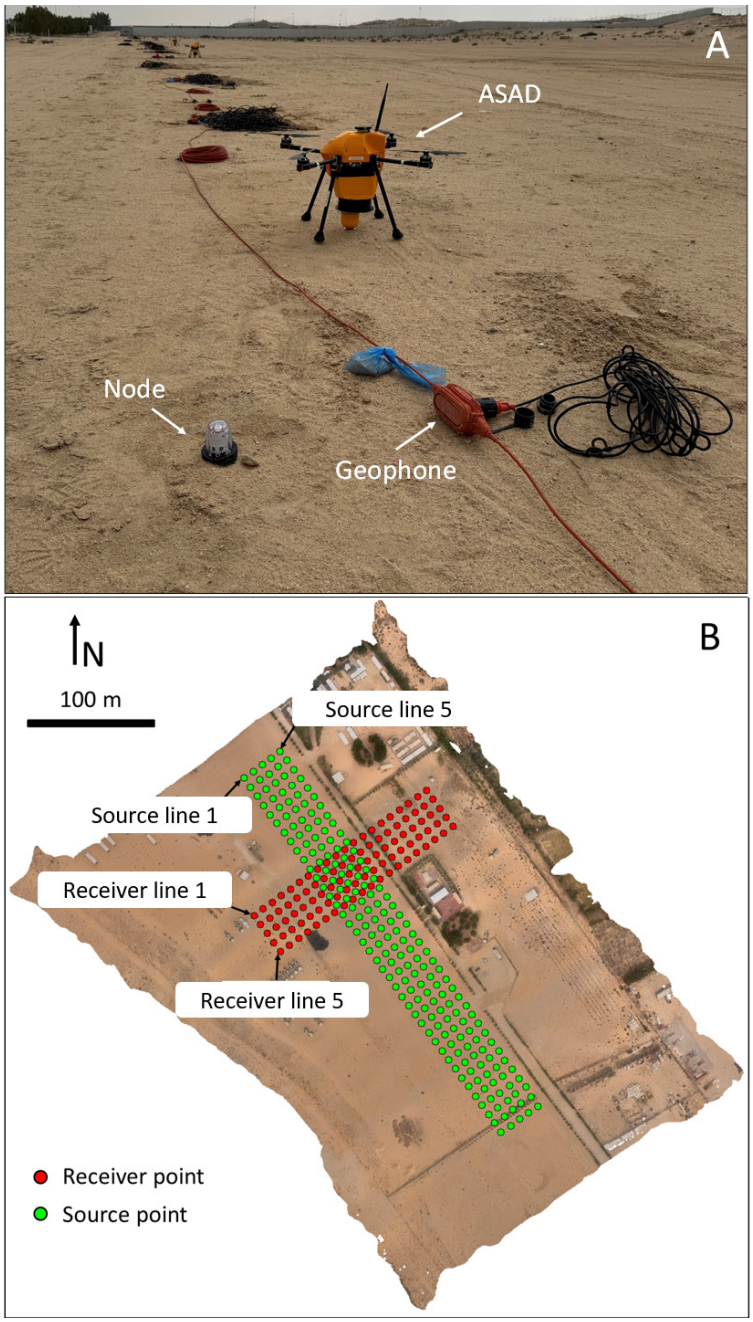

Figure 10. (**A**) Example of validation setup showing co-located ASAD acquisition points with commercial wireless nodes and conventional geophones for direct comparison of recorded seismic wavefields. (**B**) Experimental grid comprising five source lines (40 points per line) and five receiver lines (20 points per line). The ASAD swarm sequentially recorded data along each receiver line, while conventional systems remained stationary at each station.

The active seismic source for the mission was a vibroseis truck that executed an 18 s linear sweep signal from 1.5 Hz to 80 Hz. Precise synchronization between the ASAD units and the stationary conventional system was critical for data integrity. This synchronization was achieved via the ASAD's ODAM, which synchronized the recording cycle to Universal Coordinated Time (UTC) using a Pulse Per Second (PPS) signal from the onboard GNSS receiver. This architecture restricted internal clock drift to less than 0.01 ms, ensuring that the seismic signals captured by the ASAD were perfectly aligned with those recorded by the conventional nodes.

4.2. Seismic Data Processing

Once the ASAD swarm completed the mission and returned to the home position, we collected and recorded data from each UAV and processed the seismic data using the P-wave refraction tomography method [34,35] to transform raw signals into interpretable subsurface models (Figure 11). We retrieved the raw recorded data from the ASADs' onboard data acquisition modules, which were digitized at a 1 ms sampling rate prior to retrieval. The raw recorded data were then converted to SEGY-format seismograms, bandpass filtered to remove frequencies outside of the range of interest (Ormsby filter 5-10-80-100 Hz), filtered for incoherent noise, and corrected for statics to account for near-surface irregularities [36]. The seismograms across all receiver lines were sorted and compiled into a common receiver gather (CRG), which served as the foundation for first-break picking (Figure 12A). This has been performed in the commercial seismic data processing software. For the ASAD data, the workflow is the same, with the addition of prior steps of data retrieval from the drone memory and the conversion from the native binary format to SEGYs and forming CRGs according to the source timetable. We initiated the 3D refraction tomography process using first-arrival travel-time picks from the CRG [37]. The travel-time picks suggest an initial velocity model with a three-layer layout (Figure 12B). Refraction tomography was conducted with a grid factor of $2 \times 2 \times 1$ cell size with a smoothing control factor of 1, then proceeded through 20 iterations, refining the model until a final 3D velocity representation of the test area was obtained. A similar seismic data-processing workflow was applied to the conventional datasets to enable standardized comparison.

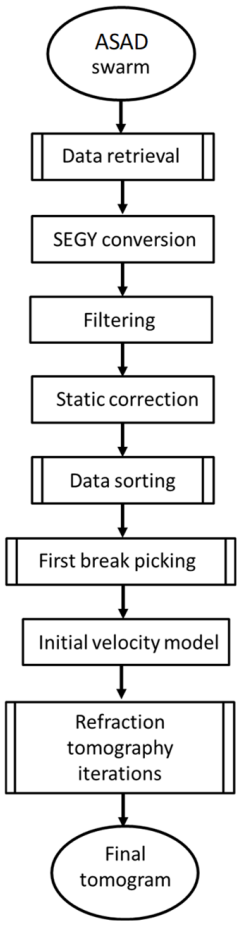

Figure 11. Seismic data processing workflow.

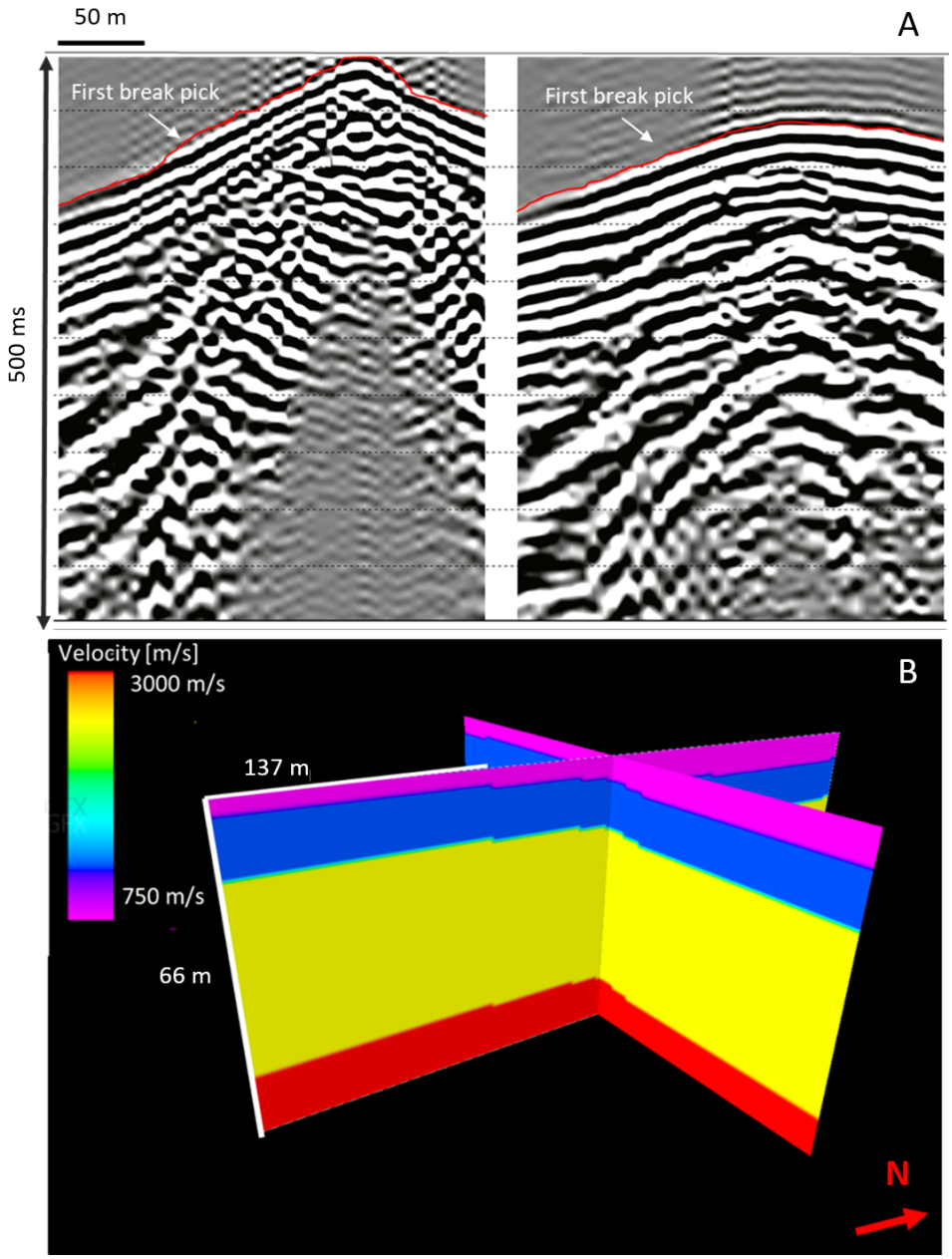

Figure 12. (**A**) Examples of ASAD's Common Receiver Gathers (CRG) for the short (**left**) and long (**right**) crossline offset used for first-break picking. The seismograms, compiled from the ASAD onboard data acquisition modules, were converted to SEGY format, filtered for noise, and corrected for statics. These picks serve as the fundamental input for the subsequent 3D refraction tomography process. (**B**) Vp-model created from initial velocity parameters of the field area.

5. Results

5.1. Mission Execution

The joint mission was successfully executed following the three-stage cooperative workflow. The Scouting UAV provided the necessary terrain intelligence, which was then converted into a semantic safe-landing map for the ASAD swarm (Figure 9). During the acquisition phase, the 20-unit ASAD swarm navigated to preplanned coordinates using RTK GNSS with centimeter-level accuracy. Once on-site, the UAVs performed a controlled descent, landed, and deployed their seismic sensors through an active coupling mechanism that utilizes their weight to ensure rigid ground contact. The transition to an "idle-ground"

state effectively eliminated mechanical noise from the rotors, providing a quiet environment for seismic recording.

5.2. Results from Seismic Data

A direct comparison of the ASAD's recorded seismic data with co-located conventional geophones demonstrates high data fidelity. The CRGs produced by the ASADs are similar in character and quality to those recorded by conventional, stationary geophones (Figure 13). The detailed analysis reveals that the ASAD data are slightly noisier due to its single-point recording versus a nine-geophone array. To ensure fair comparison, we did not apply any amplitude correction or array response compensation to any of the datasets. This similarity validates the use of seismic data processing methods to enhance the performance of lightweight UAV sensors. Frequency spectrum analysis (Figure 14) shows that the frequency bandwidth of ASAD data is superior to that of conventional geophones. ASAD data yields a wider bandwidth, especially at lower frequencies. The processed 3D refraction tomograms exhibit a three-layer architecture, with velocity boundaries and gradients across the line (Figure 15). Low-velocity near-surface layer (approx. 300–500 m/s) consistent with the loose sand and soil observed at the site, followed by more competent layers at depth. The tomogram successfully identified the signature of the artificial geohazard. The buried industrial barrel created a localized zone of reduced velocity at 2 m below the surface (Figure 15). The exact scale and shape of the anomaly are not fully captured due to its size beyond the resolution of the land seismic. It is important to note that the actual shallow cavities observed in the region are tens of meters in spatial extent and will be detected with the proposed method.

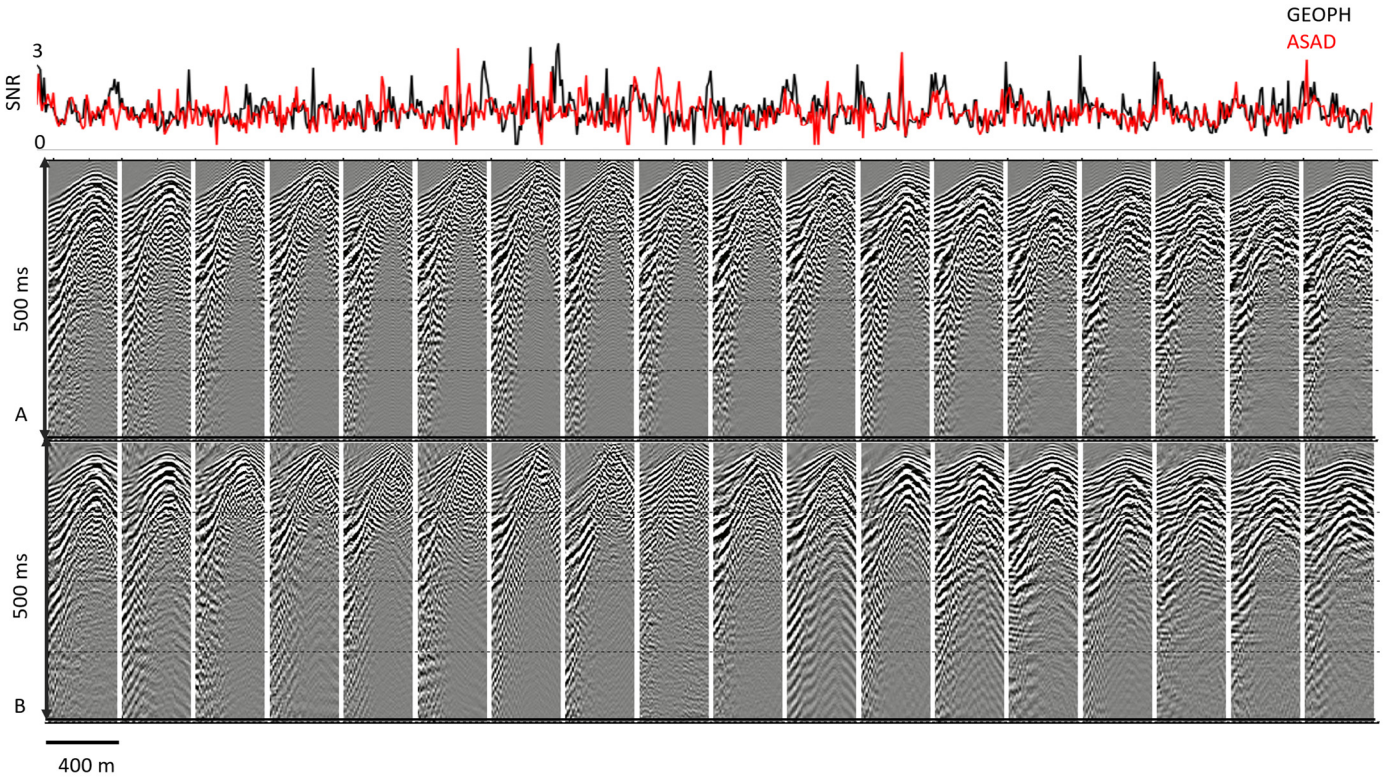

Figure 13. Comparison of Common Receiver Gathers (CRGs) between conventional geophones (**A**) and ASAD (**B**). The Signal-to-Noise Ratio (SNR) for each trace is shown in the upper plot for geophones (black) and ASAD (red). One can observe great similarity in the two datasets in terms of the general look of the wavefield, as well as very comparable SNR (geophone mean 1.21, ASAD mean 1.14).

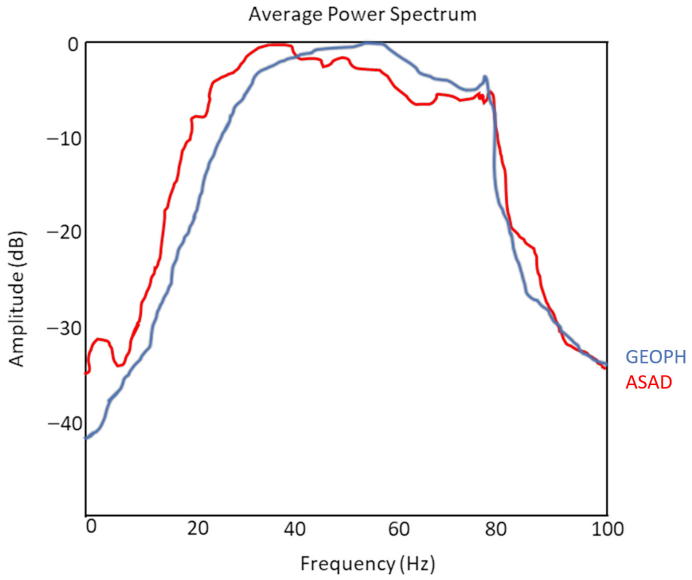

Figure 14. Frequency spectrum analysis of conventional geophones (blue) and ASAD (red). A comparison of the bandwidth between the two systems demonstrates that the ASAD data yields a wider frequency range, particularly showing superior performance at lower frequencies compared to conventional geophones.

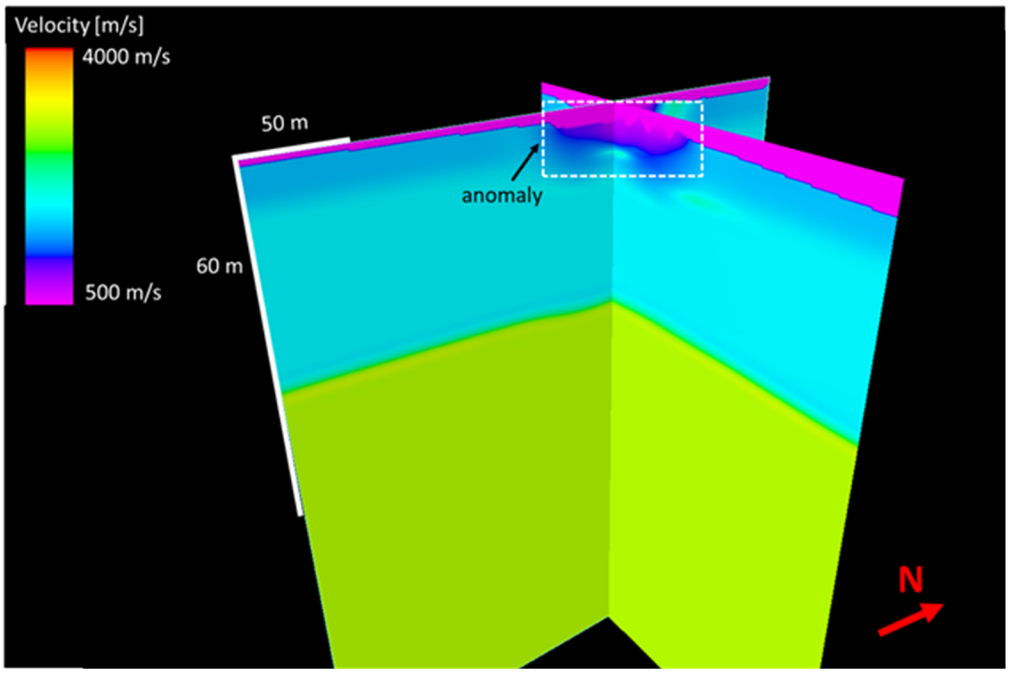

Figure 15. Refraction tomogram showing subsurface velocity structure and geohazard detection. The model illustrates a three-layer architecture, beginning with a low-velocity near-surface layer (400–500 m/s) composed of loose sand and soil. Notably, the tomogram successfully identifies the signature of the artificial geohazard as a localized zone of reduced velocity approximately 2 m below the surface.

6. Discussion

The integration of a Scouting UAV is critical to the success of autonomous missions, providing a level of detail that satellite data cannot. While satellite imagery offers a broad overview, its relatively low resolution and lack of up-to-date information often mask recent obstacles. In this trial, UAV-based photogrammetry identified buildings, trees, and tents

that were absent from satellite datasets (Figure 8G,H). These discrepancies could lead to equipment failure or safety risks if overlooked. The resulting "No-go" zone analysis map (Figure 9) directly improved mission safety. By flagging slopes greater than 15°, the system autonomously adjusted its landing coordinates to avoid hazardous terrain. This workflow ensures that every sensor is placed in an optimal landing zone, thereby maximizing field productivity while protecting the robotic assets.

A direct comparison between the CRG of the conventional geophone network and the ASAD swarm reveals distinct operational trade-offs. ASAD data showed slightly higher noise levels than the manually planted geophone arrays (Figure 13). This noise is primarily attributed to coupling variances. The human crew manually ensures firm ground contact for the conventional geophones. On the other hand, ASAD relies on its ~5 kg weight and an automated deployment mechanism to press the sensor into the terrain. However, a basic denoising applied to the ASAD data may rectify these slight discrepancies. Additionally, ASAD data yield a superior frequency bandwidth (Figure 14) compared to conventional geophones. ASAD data showcasing superior performance starting at lower frequencies may indicate a more stable and higher resolution seismic image, enabling the detection of smaller subsurface anomalies [33]. Thus, ASAD data might be better suited for imaging thinner anomalies due to potential improvements in vertical resolution.

The results of this field trial represent a successful proof-of-concept for a fully autonomous "flying sensor" ecosystem that offers distinct advantages for near-surface characterization. A critical interpretation of these findings lies in the spectral trade-off between noise and bandwidth. While ASAD data exhibits slightly higher noise due to single-point recording, it offers a wider frequency bandwidth than conventional 9-geophone arrays. Thus, making it better suited for imaging thin anomalies and improving vertical resolution.

Operationally, the fact that 100 receiver points were recorded using only 20 ASAD units through autonomous repositioning proves that robotic swarms can drastically reduce the logistical burden and manual labor associated with traditional equipment mobilization. Furthermore, the discrepancy between UAV-based photogrammetry and satellite imagery (which failed to identify recent obstacles like trees and buildings) demonstrates that high-resolution, up-to-date terrain models are an absolute prerequisite for the safe deployment of autonomous assets in arid environments. Ultimately, the successful detection of the signature of the 2 m-deep artificial cavity validates ASAD's sensitivity, establishing this cooperative workflow as a definitive tool for rapid georeconnaissance and geohazard identification in logistically complex areas.

Despite the successful field demonstration, several challenges remain for large-scale Scouting and ASAD deployment. Increasing the number of ASAD units will require more robust communication systems and sophisticated power management solutions, such as automated battery-swapping stations. Mechanical coupling remains sensitive to surface conditions (e.g., extremely loose sand or hard rock). Therefore, future iterations may require adaptive coupling mechanisms to adjust the downward force in response to real-time soil resistance or different types of coupling-independent seismic sensors. While photogrammetric processing provides high-resolution insights, it introduces a time lag between reconnaissance and acquisition. Optimizing onboard "edge" computing could eventually allow for real-time terrain analysis and landing adjustments. In contrast to the small artificial cavity used in this study, geological near-surface cavities in desert environments are typically much larger, often spanning tens of meters in width. As a result, the autonomous seismic acquisition proposed in this paper would be sufficient for more detailed imaging of these larger anomalies. Future studies will focus on testing and validating this cooperative workflow in various unknown locations.

7. Conclusions

We presented an integrated workflow for autonomous land seismic data acquisition, combining a photogrammetry UAV for site reconnaissance with seismic recording UAVs in a single cooperative mission ecosystem. The workflow consists of three stages: Reconnaissance, Planning, and Acquisition, followed by seismic processing. In a field test, a Scouting UAV generated cm-scale DEMs and an orthomosaic to guide the safe landing of ASADs, which then performed seismic acquisition. The resulting data was comparable in quality to that from conventional geophones. Refraction tomography revealed a shallow subsurface cavity reliably and comparably to traditional geophones. This innovative approach solves the "blind flight" problem. The successful recording of 100 receiver points using only 20 ASAD units through five autonomous repositioning cycles demonstrates the viability of dynamic, adaptive robotic swarming for specialized seismic data acquisition. This system achieves a frequency bandwidth comparable to industry-standard geophone arrays and reliably detects shallow subsurface cavities, confirming its readiness for field applications. By leveraging automated drone-based workflows, the system may potentially reduce acquisition cost, time, and environmental footprint, and minimize safety risk in inaccessible terrain and/or logistically complex areas of interest. This integrated robotic workflow represents a substantive scientific and engineering advance in the field of autonomous seismic acquisition.

Author Contributions: Conceptualization, P.G.; methodology, P.G., A.T. and G.Y.; software, A.T., I.M., J.A. and A.I.R.; validation, J.A., A.I.R., A.T., P.G. and G.Y.; formal analysis, J.A., A.I.R., P.G., A.T. and G.Y.; investigation, J.A., A.I.R., A.T., I.M. and G.Y.; resources, P.G. and G.Y.; data curation, J.A., A.I.R., A.T., G.Y. and P.G.; writing—original draft preparation, J.A., A.I.R. and A.T.; writing—review and editing, J.A., A.I.R., G.Y., A.T. and P.G.; visualization, J.A., A.I.R., G.Y. and A.T.; supervision, P.G. and G.Y.; project administration, P.G. and G.Y.; funding acquisition, P.G., G.Y. and E.A.; field experiment design, V.D., P.G. and A.I.R. All authors have read and agreed to the published version of the manuscript.

Funding: This research received no external funding.

Data Availability Statement: Data associated with this research are confidential and cannot be released.

Conflicts of Interest: J.A., A.I.R., P.G., and E.A. were employed by EXPEC Advanced Research Center, Saudi Aramco; A.T., G.Y., and I.M. were employed by Aramco Innovations LLC; V.D. was employed by the Geophysical Imaging Department, Saudi Aramco. The remaining authors declare that the research was conducted in the absence of any commercial or financial relationships that could be construed as a potential conflict of interest.

References

1. Chopra, S.; Marburg, K.J. *Seismic Attributes for Prospect Identification and Reservoir Characterization*; Society of Exploration Geophysicists and European Association of Geoscientists and Engineers: Houston, TX, USA, 2007.
2. Pegah, E.; Liu, H. Application of near-surface seismic refraction tomography and multichannel analysis of surface waves for geotechnical site characterizations: A case study. *Eng. Geol.* **2016**, *208*, 100–113. [CrossRef]
3. Bruno, P.P.G. Seismic exploration methods for structural studies and for active fault characterization: A review. *Appl. Sci.* **2023**, *13*, 9473. [CrossRef]
4. Ourabah, A.; Chatenay, A. Unlocking ultra-high-density seismic for CCUS applications by combining nimble nodes and agile source technologies. *Lead. Edge* **2022**, *41*, 27–33. [CrossRef]
5. Ourabah, A.; Keggin, J.; Brooks, C.; Ellis, D.; Etgen, J. Seismic Acquisition, What Really Matters? In Proceedings of the 2015 SEG Annual Meeting, New Orleans, LA, USA, 18–23 October 2015.
6. Chopra, S.; Larsen, G. Acquisition footprint—Its detection and removal. *CSEG Rec.* **2000**, *25*, 16–20.
7. Ramdani, A.I.; Golikov, P.; Alsoqair, K.; Serpiva, V.; Alfataierge, E. On-demand high-resolution areal scouting via unmanned aerial vehicles enables sustainable near-surface geoscience data acquisition. *Lead. Edge* **2024**, *43*, 494–505. [CrossRef]

8. Deng, Z. 3D seismic acquisition in a complex mountainous area. *J. Geophys. Eng.* **2004**, *1*, 17–27. [CrossRef]
9. Dieulangard, D.; Popham, M.; Grant, C.; O'Connell, K.; Ourabah, A.; Einchcomb, C. Land seismic recording systems in a changing world—A 2021 review. *First Break* **2022**, *40*, 59–65. [CrossRef]
10. Laake, A. Seismic logistics and planning. In *Remote Sensing for Hydrocarbon Exploration*; Laake, A., Ed.; Springer Nature: Cham, Switzerland, 2022; pp. 189–224.
11. Laake, A.; Insley, M. Applications of satellite imagery to seismic survey design. *Lead. Edge* **2004**, *23*, 1062–1064. [CrossRef]
12. Colombo, D.; Sandoval-Curiel, E.; Alyousuf, T.; Turkoglu, E.; Rovetta, D. Ultra-dense nodal seismic acquisition for automated geohazard analysis. *Lead. Edge* **2024**, *43*, 484–493. [CrossRef]
13. Lys, P.-O.; Elder, K.; Archer, J.; Team, M. METIS, a disruptive R&D project to revolutionize land seismic acquisition. In Proceedings of the Research and Development Petroleum Conference and Exhibition 2018, Abu Dhabi, United Arab Emirates, 9–10 May 2018; pp. 28–31.
14. Masoni, I.; Pagliccia, B.; Thalmann, G. The Use of Drones for Innovative Seismic Acquisition: A Change of Paradigm for HSE. In Proceedings of the International Petroleum Technology Conference, Beijing, China, 27–29 March 2019.
15. Wu, X.; Xue, G.-Q.; Wang, Y.-B.; Cui, S. Current Progress in and Future Visions of Key Technologies of UAV-Borne Multi-Modal Geophysical Exploration for Mineral Exploration: A Scoping Review. *Remote Sens.* **2025**, *17*, 2689. [CrossRef]
16. Dadrass Javan, F.; Samadzadegan, F.; Toosi, A.; van der Meijde, M. Unmanned Aerial Geophysical Remote Sensing: A Systematic Review. *Remote Sens.* **2025**, *17*, 110. [CrossRef]
17. Shahsavani, H.; Smith, R.S. Aeromagnetic gradiometry with UAV, a case study on small iron ore deposit. *Drone Syst. Appl.* **2024**, *12*, 1–9. [CrossRef]
18. Junaid, M.; Al-Atroush, M.E.; Mahmood, S.; Sultan Shah, K.; Ullah, A. Recent developments in unmanned aerial vehicle (UAV) surveys for rock slope stability analysis—A review. *Geocarto Int.* **2025**, *40*, 2519915. [CrossRef]
19. Yashin, G.; Serpiva, V.; Timoshenko, A.; Mikhailovskiy, N.; Egorov, A.; Golikov, P. ASAD: Autonomous Seismic Acquisition Device. *Int. J. Control. Autom. Syst.* **2023**, *21*, 2464–2475. [CrossRef]
20. Sudarshan, S.K.; Huang, L.; Li, C.; Stewart, R.; Becker, A.T. Seismic surveying with drone-mounted geophones. In Proceedings of the 2016 IEEE International Conference on Automation Science and Engineering (CASE), Fort Worth, TX, USA, 21–25 August 2016; pp. 1354–1359.
21. Timoshenko, A.; Yashin, G.; Serpiva, V.; Hamadov, R.; Fedotov, D.; Kartashova, M.; Golikov, P. Seismic Data Acquisition Utilizing a Group of UAVs. *Drones* **2025**, *9*, 156. [CrossRef]
22. Maxar. Maxar Vivid Imagery. World Imagery 2019. Available online: https://www.arcgis.com/apps/mapviewer/index.html?webmap=c03a526d94704bfb839445e80de95495 (accessed on 7 April 2026).
23. Alkhalifa, M.A.; Kurison, C. Karst collapse and gypsum-filled veins in Eocene outcrops, Dammam Dome, Saudi Arabia: Causes and implications. *Geosyst. Geoenviron.* **2023**, *2*, 100109. [CrossRef]
24. Bačić, M.; Librić, L.; Kaćunić, D.J.; Kovačević, M.S. The Usefulness of Seismic Surveys for Geotechnical Engineering in Karst: Some Practical Examples. *Geosciences* **2020**, *10*, 406. [CrossRef]
25. Amin, A.A.; Bankher, K.A. Karst hazard assessment of eastern Saudi Arabia. *Nat. Hazards* **1997**, *15*, 21–30. [CrossRef]
26. Cueto, M.; Olona, J.; Fernández-Viejo, G.; Pando, L.; López-Fernández, C. Karst-induced sinkhole detection using an integrated geophysical survey: A case study along the Riyadh Metro Line 3 (Saudi Arabia). *Near Surf. Geophys.* **2018**, *16*, 270–281. [CrossRef]
27. Youssef, A.M.; El-Kaliouby, H.M.; Zabramawi, Y. Integration of remote sensing and electrical resistivity methods in sinkhole investigation in Saudi Arabia. *J. Appl. Geophys.* **2012**, *87*, 23–39. [CrossRef]
28. Al-Halbouni, D.; Holohan, E.P.; Taheri, A.; Schöpfer, M.P.; Emam, S.; Dahm, T. Geomechanical modelling of sinkhole development using distinct elements: Model verification for a single void space and application to the Dead Sea area. *Solid Earth* **2018**, *9*, 1341–1373. [CrossRef]
29. Pinton, D.; Canestrelli, A.; Moon, R.; Wilkinson, B. Estimating ground elevation in coastal dunes from high-resolution UAV-LIDAR Point Clouds and Photogrammetry. *Remote Sens.* **2022**, *15*, 226. [CrossRef]
30. Westoby, M.J.; Brasington, J.; Glasser, N.F.; Hambrey, M.J.; Reynolds, J.M. 'Structure-from-Motion'photogrammetry: A low-cost, effective tool for geoscience applications. *Geomorphology* **2012**, *179*, 300–314. [CrossRef]
31. Nex, F.; Remondino, F. UAV for 3D mapping applications: A review. *Appl. Geomat.* **2014**, *6*, 1–15. [CrossRef]
32. Al-Kaff, A.; Gómez-Silva, M.J.; Moreno, F.M.; De La Escalera, A.; Armingol, J.M. An appearance-based tracking algorithm for aerial search and rescue purposes. *Sensors* **2019**, *19*, 652. [CrossRef] [PubMed]
33. Martínez-Carricondo, P.; Agüera-Vega, F.; Carvajal-Ramírez, F.; Mesas-Carrascosa, F.-J.; García-Ferrer, A.; Pérez-Porras, F.-J. Assessment of UAV-photogrammetric mapping accuracy based on variation of ground control points. *Int. J. Appl. Earth Obs. Geoinf.* **2018**, *72*, 1–10. [CrossRef]
34. White, D.J. Two-Dimensional Seismic Refraction Tomography. *Geophys. J. Int.* **1989**, *97*, 223–245. [CrossRef]

35. Lanz, E.; Maurer, H.; Green, A.G. Refraction tomography over a buried waste disposal site. *Geophysics* **1998**, *63*, 1414–1433. [CrossRef]
36. Marsden, D. Static corrections—A review, Part II. *Lead. Edge* **1993**, *12*, 115–120. [CrossRef]
37. Zelt, C.A.; Barton, P.J. Three-dimensional seismic refraction tomography: A comparison of two methods applied to data from the Faeroe Basin. *J. Geophys. Res. Solid Earth* **1998**, *103*, 7187–7210. [CrossRef]

Disclaimer/Publisher's Note: The statements, opinions and data contained in all publications are solely those of the individual author(s) and contributor(s) and not of MDPI and/or the editor(s). MDPI and/or the editor(s) disclaim responsibility for any injury to people or property resulting from any ideas, methods, instructions or products referred to in the content.